BNL-107019-2014-TECH
C-A/AP/531;BNL-107019-2014-IR

9-D polarized proton transport in the MEIC 'figure -8' collider ring - first steps

F. Meot

October 2014

Collider Accelerator Department
Brookhaven National Laboratory

U.S. Department of Energy
USDOE Office of Science (SC), Nuclear Physics (NP) (SC-26)

DISCLAIMER

BNL-107019-2014-IR

C-A/AP/531
October 2014

9-D Polarized proton transport in the MEIC "figure-8" collider ring – first steps

F. Méot, V.S. Morozov

Collider-Accelerator Department
Brookhaven National Laboratory
Upton, NY 11973

U.S. Department of Energy
Office of Science, Office of Nuclear Physics

9-D polarized proton transport in the MEIC "figure-8" collider ring - first steps

F. Méot and V.S. Morozov

BNL C-AD, Upton, LI, NY, and JLab, Newport News, Va

October 27, 2014

Abstract

Spin tracking studies in the MEIC figure-8 collider ion ring are presented, based on a very preliminary design of the lattice. They provide numerical illustrations of some of the aspects of the figure-8 concept, including spin-rotator based spin control, and lay out the path towards a complete spin tracking simulation of a figure-8 ring.

Tech. Note C-A/AP/531 (2014)

Contents

1 Introduction

Proton spin tracking studies in the 60 GeV figure-8 ring of the MEIC electron-ion collider (Fig. 1) are presented here. Table 1 summarizes the nominal parameters of the ring, details can be found in [1].

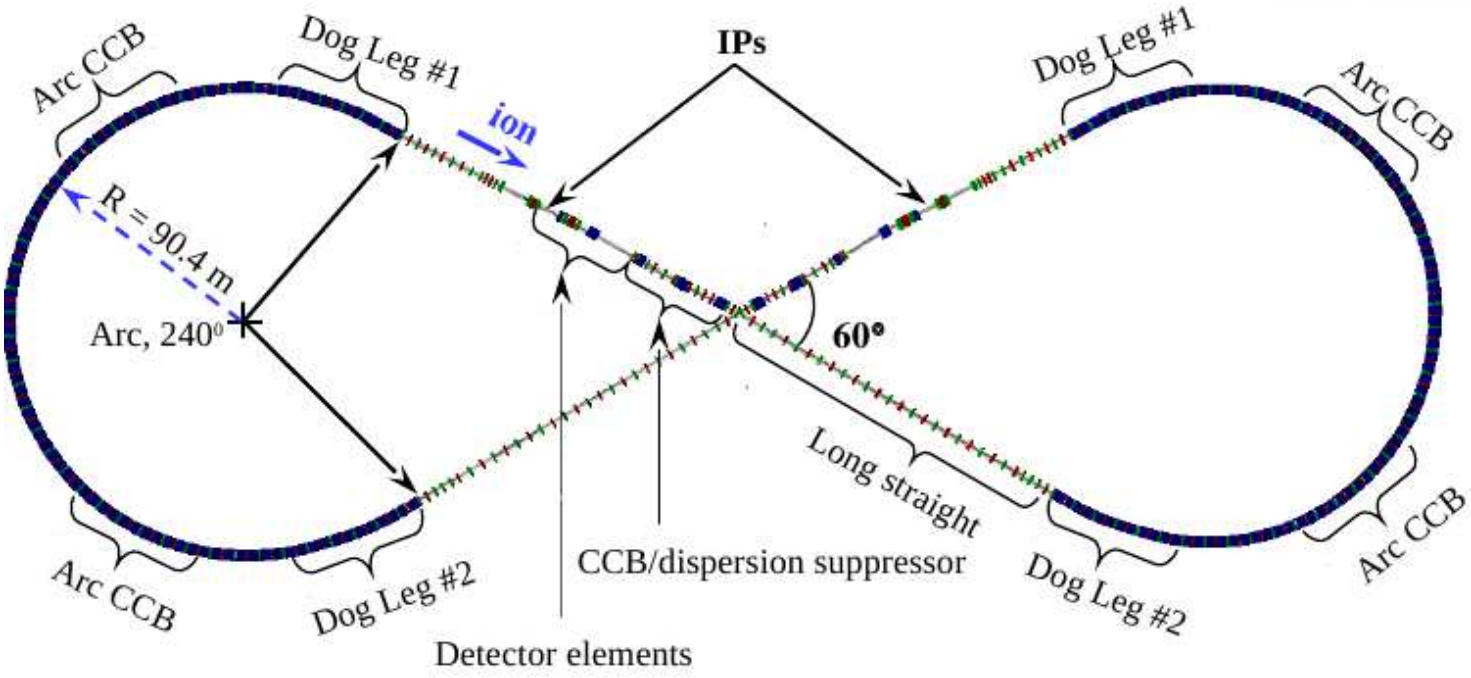

Figure 1: MEIC collider ion ring.

Table 1: Parameters of the 60 GeV MEIC figure 8 collider proton ring. Tracking outcomes, see Figs. 4-6, are added for comparison (column 4).

circumference	m	1415.3	
energy	GeV	60	
polarization	%	>70	
horizontal/vertical emittances, normalized	$\pi\mu$m.rad	0.35 / 0.07	
horizontal/vertical β^*	cm	10 / 2	10.0 / 2.0
max. β_x / β_y	m	2301 / 2450	2303 / 2451
horizontal/vertical tunes		25.79 / 26.27	25.790 / 26.260
horizontal/vertical chromaticities, natural		-224 / -233	-223 / -233
momentum compaction	10^{-3}	5.76	5.30
transition γ		13.18	13.74

These studies were done using a very preliminary design of the lattice, however not optimized for the spin dynamics and in particular not including the system intended for polarization control in MEIC. They can be viewed as simplified numerical illustrations of some of the aspects of the figure-8 concept on the one hand, and on the other hand they lay out the path towards a complete spin tracking simulation of a figure-8 ring.

In view of serving as a guidance in further use of the simulation material, this report discusses various aspects of the tracking code used, Zgoubi [2], including the content of the input data files and some methods proper to stepwise ray-tracing. A preliminary Zgoubi input data file has been obtained from translation of a MADX “twiss” file, using MADX2Zgoubi translator [3], an excerpt is given in appendix, page 12.

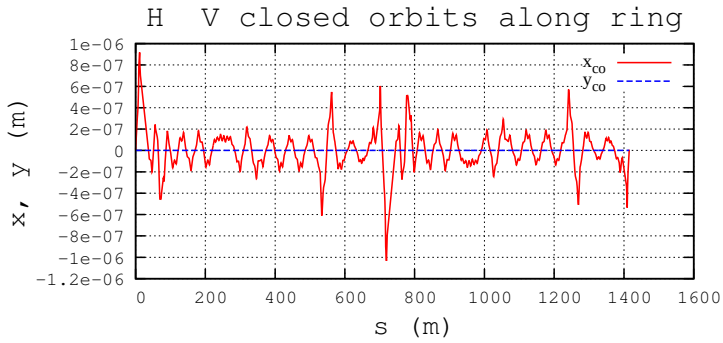

Figure 2: Closed orbits, horizontal and vertical. The horizontal orbit is not exactly zero, since the ray-tracing restitutes with finite accuracy the exact arc of a circle that the trajectory does in a constant field dipole.

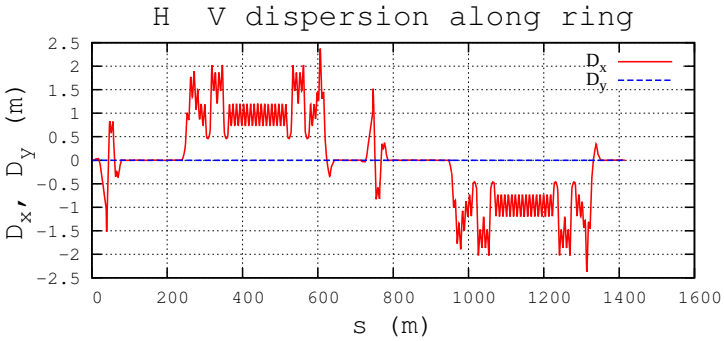

Figure 3: Dispersion functions, horizontal and vertical.

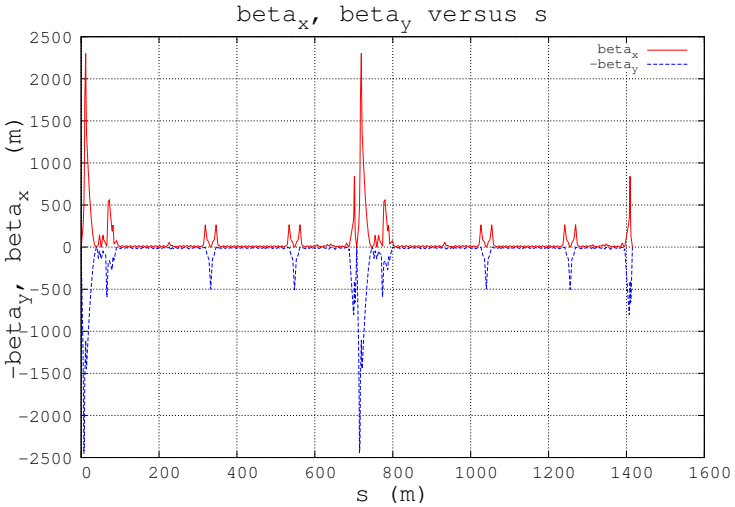

Figure 4: Optical functions, horizontal and vertical.

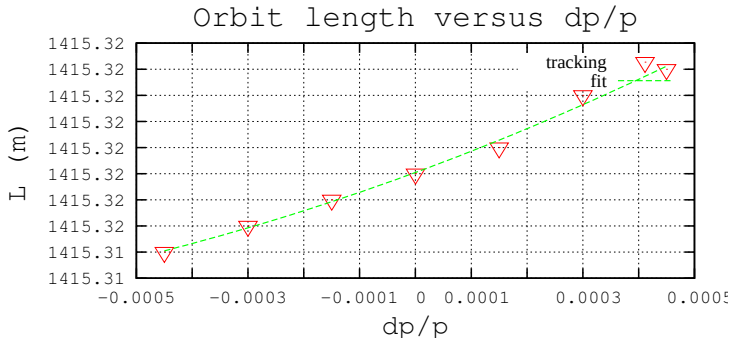

Figure 5: Momentum dependence of orbit length.

$L_0 = 1415.3207$, $\gamma_{tr} = 13.737155$, $\alpha_0 = 5.29915234 \times 10^{-3}$, $\alpha_1 = 1.2617025$, $\alpha_2 = 6.95625669 \times 10^{-4}$

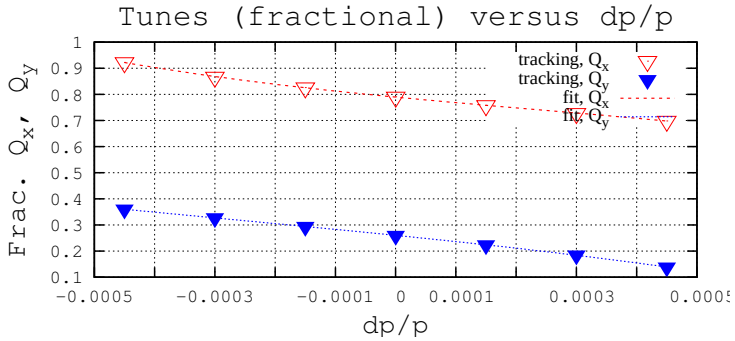

Figure 6: Momentum dependence of tunes, and matching polynomials $Q(\delta) = Q_0 + Q'\delta + Q''\delta^2 + Q'''\delta^3$.

Horizontal : $Q_x = 0.79044700$, $Q'_x = -223.10913$, $Q''_x = 91688.195$
Vertical : $Q_y = 0.26025653$, $Q'_y = -233.28488$, $Q''_y = -49249.980$

2 Ring optics

This section summarizes paraxial optical data as obtained from preliminary tracking exercises, as well as various long-term tracking considerations relevant to polarization transport simulations.

2.1 Optical parameters

The ring lattice is linear at the present stage - no sextupoles, in particular. Hard edge field models are used, however fringe fields may be introduced for modeling accuracy, if considered useful.

In the following the optical functions are reported, for reference, they can be compared to the nominal data in table 1.

Orbits, horizontal and vertical, are first searched, Fig. 2. This can be performed either using the "searchCO" tool from Zgoubi toolbox [3] (a usual multi-turn technique), or using a self-consistent input data file based on Zgoubi's '`FIT`' procedure. The vertical orbit is zero in the present case (although the actual lattice does include four vertical localized, short bumps).

The dispersion functions, $D_x(s)$, $D_y(s)$, Fig. 3, can be computed using various methods, for instance,

- by transporting the periodical functions, prior determined at the origin of the optical structure (by the former "searchCO", for instance), the "`OPTICS`"command does that [2],

- by difference between paraxial chromatic orbits, using the "getDiffFromFai" tool [3].

Tunes, Fig. 6, can be determined from first order mapping or from multi-turn Fourier analysis.

Note that the "searchChroma" tool [3] will produce all of the above, including Figs. 2-6, in one go.

2.2 Long-term tracking

Tracking at constant energy is addressed in section 3, up to 200,000 turns. Figure 13 provides a sample of conservation of the invariants. The main control knob in that is the integration step size, its value being a compromise between tracking accuracy and CPU time. The latter amounts in the present conditions to about 20 turns per second, on a 1.5 GHz CPU (independent of particle number on a CPU cluster), a matter of about 3 hours in such exercises as addressed in Fig. 13.

Tracking in the presence of acceleration, up to 400,000 turns, is addressed in section 3.4. The integration step size used has to ensure that the damping do follow the evolution of beam momentum.

3 Spin tracking

The spin tracking studies presented below were done using a preliminary design of the MEIC figure-8 ion collider ring lattice. The lattice did not include the system intended for polarization control in MEIC and was not optimized for the spin dynamics. The choice of parameters used in the simulations was completely arbitrary. Therefore, these simulations do not represent a systematic study of a realistic case but should be viewed as simplified numerical illustrations of some of the aspects of the figure-8 concept. However, these results do contain the main necessary ingredients of and lay out the path towards a complete spin tracking simulation of a figure-8 ring.

3.1 Particle with zero initial coordinates in an ideal figure 8

We start by tracking three particles with zero initial coordinates and with fully longitudinal $(S_x^i = 1)$, radial $(S_y^i = 1)$, and vertical $(S_z^i = 1)$ initial spin orientations, respectively, for 200,000 turns through an ideal lattice containing no imperfections.

The following is an excerpt of the related input data list to Zgoubi in this particular exercise, for the record.

```
Generated by MADX -> Zgoubi translator
'OBJET'                                                                                    0
200138.457119         reference rigidity (kG.cm) =  60000000000.0000  ,  G.gamma =         114.6618
2
3  1
.0 .0 .0 .0 0.  1.  'o'
.0 .0 .0 .0 0.  1.  'o'
.0 .0 .0 .0 0.  1.  'o'
1 1 1
'PARTICUL'                                                                                 1
9.3827203E+02 1.602176487E-19 1.7928474 0 0
'SPNTRK'                                                                                   2
4
1. 0. 0.
0. 1. 0.
0. 0. 1.
...
'REBELOTE'                                                                              1023
199999 0.2 99
'END'                                                                                   1024
```

Figures 7 through 9 show the non-zero spin components of the three particles every 100 turns versus the turn number. Each of the different spin orientations remains the same from turn to turn as expected in a figure-8 ring. This validates the applicability of Zgoubi to this kind of study and demonstrates that it has the necessary numerical precision at least at the level of the chosen number of turns.

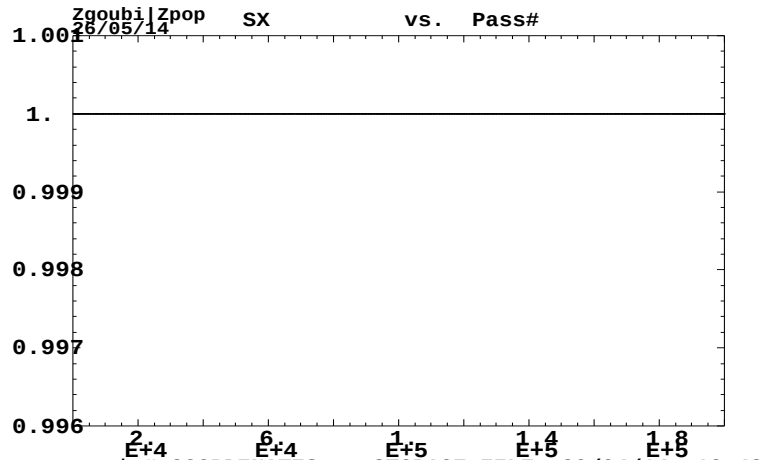

Figure 7: Longitudinal spin component S_x of the first $(S_x^i = 1)$ particle plotted vs. the turn number every 100 turns. The particle moves along the reference orbit in an ideal ring.

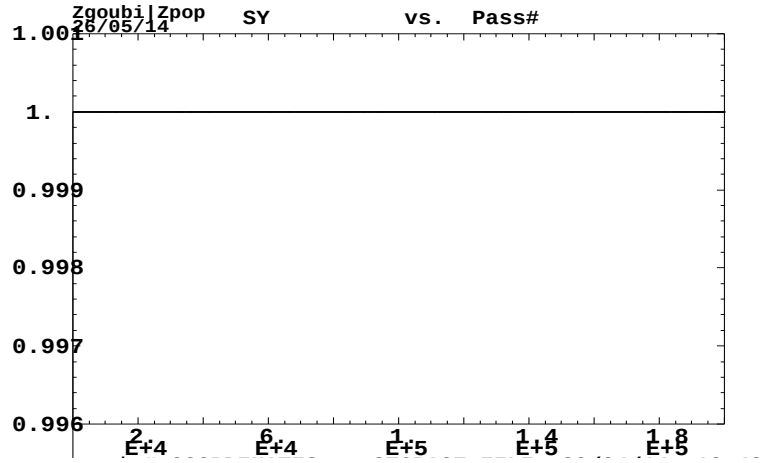

Figure 8: Radial spin component S_y of the second $(S_y^i = 1)$ particle plotted vs. the turn number every 100 turns. The particle moves along the reference orbit in an ideal ring.

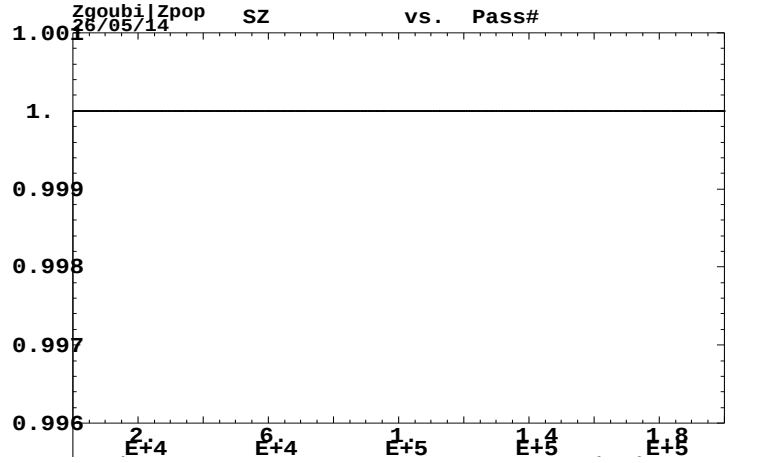

Figure 9: Vertical spin component S_z of the third $(S_z^i = 1)$ particle plotted vs. the turn number every 100 turns. The particle moves along the reference orbit in an ideal ring.

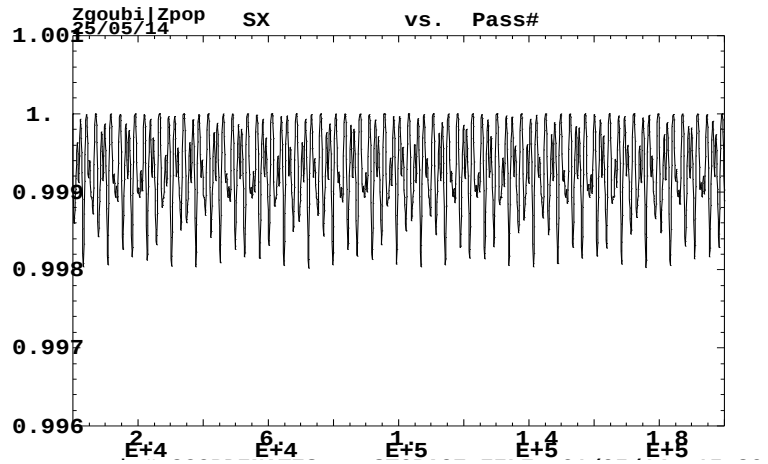

Figure 10: Longitudinal spin component S_x of the first $(S_x^i = 1)$ particle plotted vs. the turn number every 100 turns with individual points connected by a solid line. The particle is launched with initial horizontal and vertical angles both of 0.2 mrad in an ideal ring.

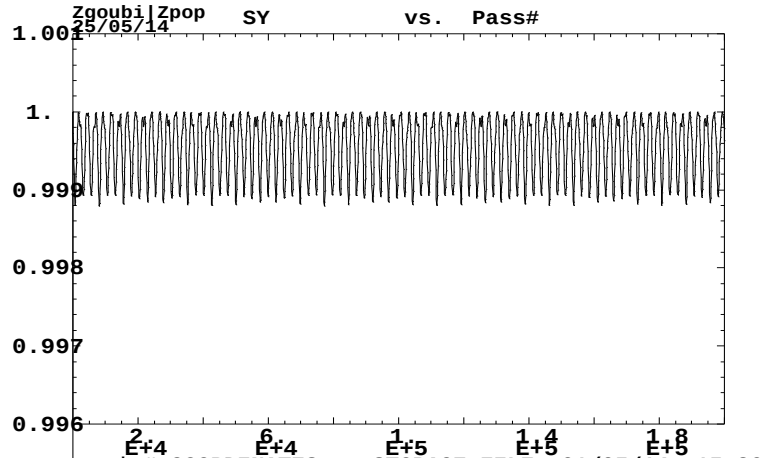

Figure 11: Radial spin component S_y of the second $(S_y^i = 1)$ particle plotted vs. the turn number every 100 turns with individual points connected by a solid line. The particle is launched with initial horizontal and vertical angles both of 0.2 mrad in an ideal ring.

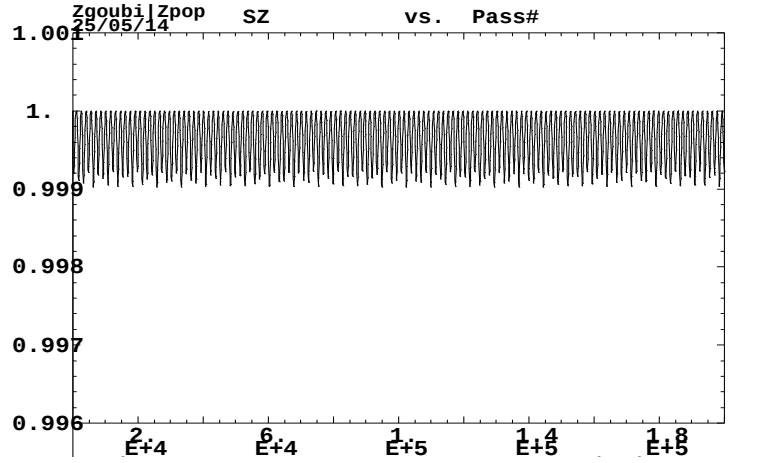

Figure 12: Vertical spin component S_z of the third $(S_z^i = 1)$ particle plotted vs. the turn number every 100 turns with individual points connected by a solid line. The particle is launched with initial horizontal and vertical angles both of 0.2 mrad in an ideal ring.

3.2 Effect of the betatron oscillations on the particle spin dynamics in an ideal figure 8

We next launch three particles from one of the MEIC interaction points (IPs), with all three different initial spin orientations, and with initial horizontal and vertical angles both of 0.2 mrad, which corresponds approximately to rms horizontal and vertical angular spreads. The particles are tracked for 200,000 turns and their main spin components are plotted every 100 turns in Figs. 10 through 12. The figures indicate that, for this order of the number of turns and still without lattice errors, there is no significant effect of the betatron oscillations on the spin motion in the figure 8 ring. Note that Figs. 7-12 all have the same scales.

```
Generated by MADX -> Zgoubi translator
'OBJET'                                                                                    0
200138.457119         reference rigidity (kG.cm) =  60000000000.0000  ,  G.gamma =         114.6618
2
3  1
.0 .2 .0 .2 0.  1.  'o'
.0 .2 .0 .2 0.  1.  'o'
.0 .2 .0 .2 0.  1.  'o'
1 1 1
'PARTICUL'                                                                                 1
9.3827203E+02 1.602176487E-19 1.7928474 0 0
'SPNTRK'                                                                                   2
4
1. 0. 0.
0. 1. 0.
0. 0. 1.
...
'REBELOTE'                                                                              1023
199999 0.2 99
'END'                                                                                   1024
```

Figure 13 shows the horizontal and vertical phase-space trajectories. The trajectories are consistent with the linear optics parameters at the observation point, the IP. Note that there is no smearing of the trajectories, which is an indication that there is no symplecticity violation in Zgoubi, at least, at this level of the number of turns.

3.3 Misalignment effects

The spin motion in a figure-8 ring by itself is not stable because of the zero-harmonic imperfection spin resonance. The main contributions to the strength of this resonance come from the dipole roll and vertical quadrupole alignment errors [4]. Therefore, below we simulate the effects of these two types of errors and their compensation.

3.3.1 Dipole roll error

Suppose that longitudinal beam polarization is required at the IP, which happens to be the particle launch location in our simulations. We introduce an imperfection in the lattice by rolling one of the arc dipoles by 0.2 mrad. Note that we do not then correct the closed orbit (essentially vertical, Fig. 14). We track a particle with initially longitudinal spin direction for 200,000 turns. The particle is launched along the reference orbit. Note, however, that it still undergoes betatron oscillations due to the closed orbit distortion. The evolution of the particle's longitudinal spin component is plotted versus the turn number every 100 turns in Fig. 15.

```
Generated by MADX -> Zgoubi translator
'OBJET'                                                                                    0
200138.457119         reference rigidity (kG.cm) =  60000000000.0000  ,  G.gamma =         114.6618
2
1  1
.0 .0 .0 .0 0.  1.  'o'
1
'PARTICUL'                                                                                 1
9.3827203E+02 1.602176487E-19 1.7928474 0 0
'SPNTRK'                                                                                   2
4
1. 0. 0.
...
'BEND'     SBEN      BARC                                 # misaligned (rolled) arc dipole                  152
0  .Bend
   2.999664890E+02   0.000200000E+00   1.725936705E-01       # skew angle of 0.2 mrad
  0.00  0.00   0.00000000
4 .2401  1.8639  -.5572  .3904 0. 0. 0.
  0.00  0.00   0.00000000
4 .2401  1.8639  -.5572  .3904 0. 0. 0.
#200|299|200    Bend  BARC
3 0. 0.    -2.588905E-02
...
'REBELOTE'                                                                              1023
199999 0.2 99
'END'                                                                                   1024
```

Clearly, the longitudinal polarization direction is not preserved at the IP in Fig. 15. To correct for this effect of the dipole roll error, we install a zero-length spin rotator at the start of the lattice, which rotates the spin by 1° about the longitudinal axis but does not affect the orbital motion. Note that such a spin rotator can be installed anywhere in the experimental straight where the polarization is longitudinal. The dynamics of the longitudinal spin component in the presence of the spin rotator is presented in Fig. 16.

```
...
'SPINR'
1
0.  1.
...
```

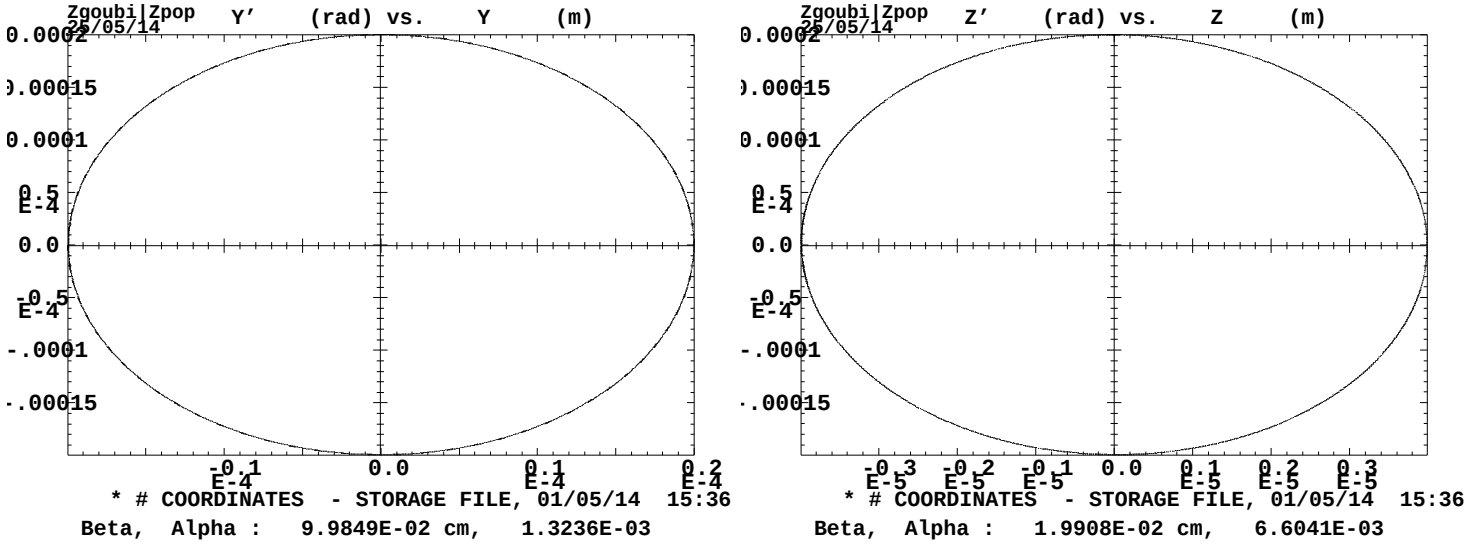

Figure 13: Horizontal (left) and vertical (right) phase-space trajectory of the particle launched with initial horizontal and vertical angles both of 0.2 mrad in an ideal ring. The phase-space points are plotted every 100 turns, over 2×10^5 turns. The matched β^* values are given at the bottom of the figure, consistent with data at the IP in table 1.

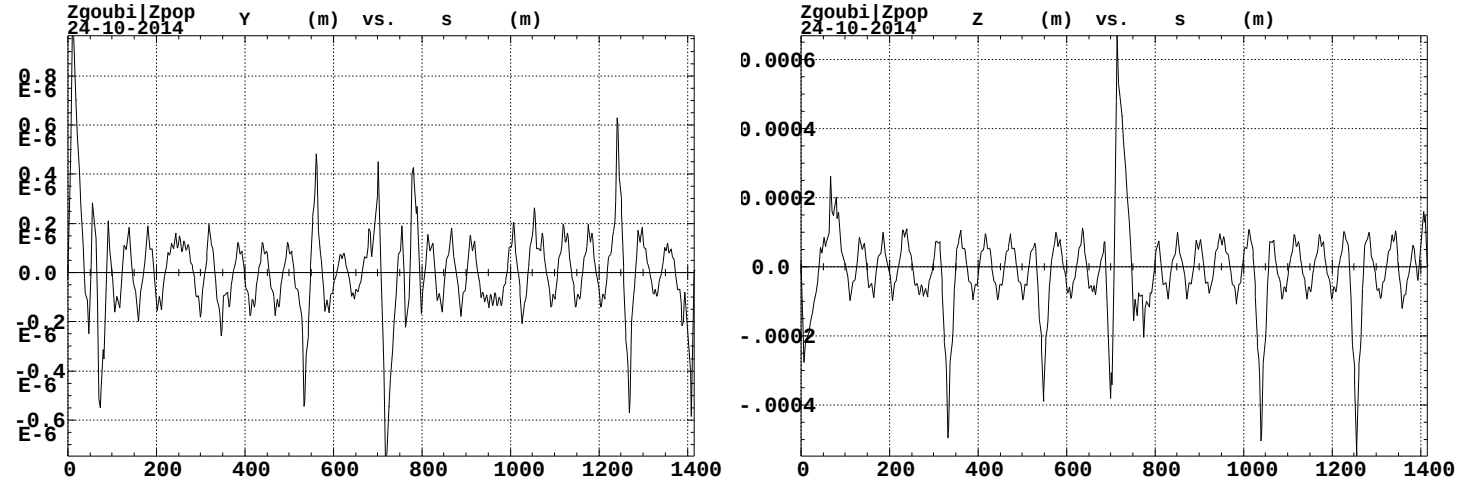

Figure 14: Closed orbits, horizontal and vertical, in the presence of a 0.2 mrad roll angle in an arc dipole.

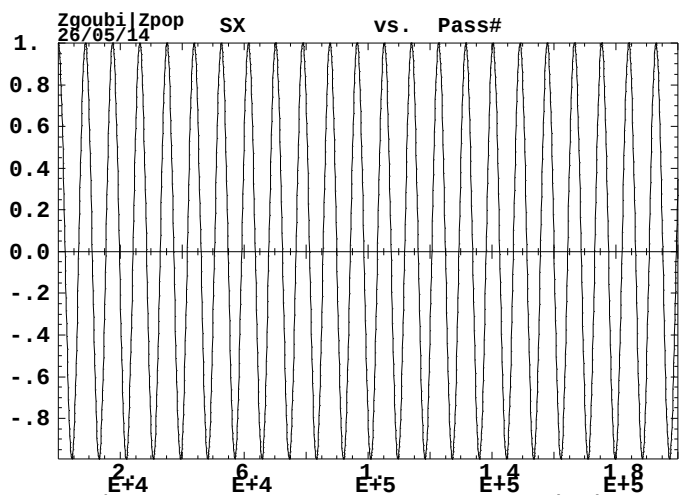

Figure 15: Longitudinal spin component S_x of the particle with $S_x^i = 1$ plotted vs. the turn number every 100 turns with individual points connected by a solid line. The particle is initially launched along the reference orbit in a ring with one of the arc dipoles rolled by 0.2 mrad.

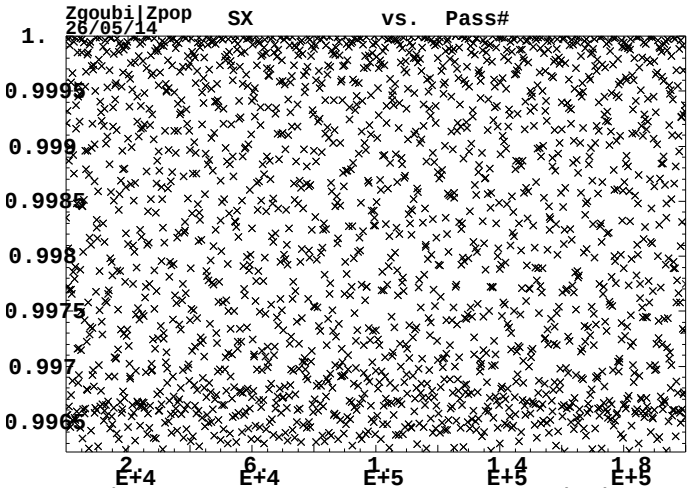

Figure 16: Longitudinal spin component S_x of the particle with $S_x^i = 1$ plotted vs. the turn number every 100 turns. The particle is initially launched along the reference orbit in a ring with one of the arc dipoles rolled by 0.2 mrad. The ring contains a spin rotator placed at the launch point, which rotates the spin by 1° about the longitudinal axis.

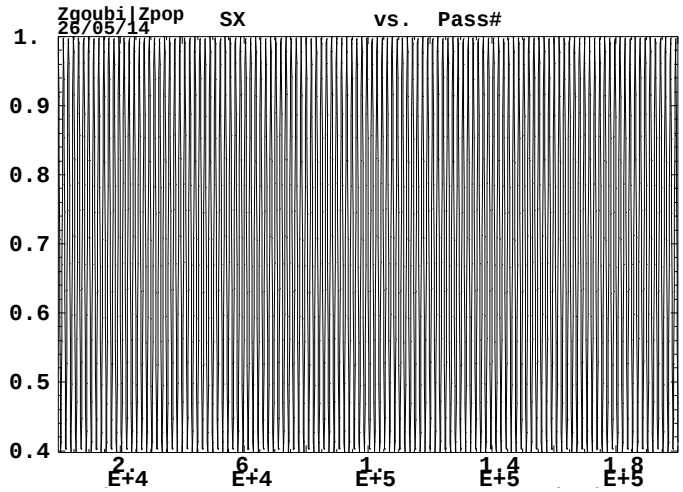

Figure 17: Longitudinal spin component S_x of the particle with $S_x^i = 1$ plotted vs. the turn number every 100 turns with individual points connected by a solid line. The particle is initially launched along the reference orbit in a ring with one of the arc quadrupoles misaligned vertically by 10 μm.

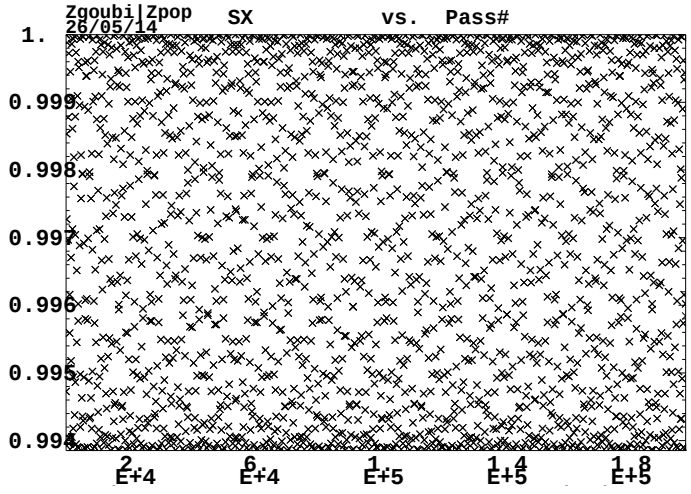

Figure 18: Longitudinal spin component S_x of the particle with $S_x^i = 1$ plotted vs. the turn number every 100 turns. The particle is initially launched along the reference orbit in a ring with one of the arc quadrupoles misaligned vertically by 10 μm. The ring contains a spin rotator placed at the launch point, which rotates the spin by 2° about the longitudinal axis.

3.3.2 Vertical quadrupole alignment error

We next do a similar study of the effect of the vertical quadrupole alignment error. We misalign one of the arc quadrupoles vertically by 10 μm. We then track a particle with initially longitudinal spin direction launched along the reference orbit for 200,000 turns. The resulting behavior of the longitudinal spin component as a function of the turn number is shown in Fig. 17.

```
Generated by MADX -> Zgoubi translator
'OBJET'                                                                                                  0
200138.457119         reference rigidity (kG.cm) =  60000000000.0000  ,  G.gamma =         114.6618
2
1  1
.0 .0 .0 .0 0.  1.  'o'
1
'PARTICUL'                                                                                               1
9.3827203E+02 1.602176487E-19 1.7928474 0 0
'SPNTRK'                                                                                                 2
4
1. 0. 0.
...
'CHANGREF'
ZS 0.001                      # introduce vertical offset in cm
'MULTIPOL' QUAD      QMQB     # 0.01 mm vertically misaligned quadrupole                                 170
0  .Quad
   50.000000 10.00    0.0000000000   -0.4426033548 0.0 0.0 0.0 0.0 0.0 0.0 0.0 0.0
0. 0. 6.00  3.00 1.00 0.00 0.00 0.00 0.00 0. 0. 0.
6  .1122 6.2671 -1.4982 3.5882 -2.1209 1.723
0. 0. 6.00  3.00 1.00 0.00 0.00 0.00 0.00 0. 0. 0.
6  .1122 6.2671 -1.4982 3.5882 -2.1209 1.723
 0. 0. 0. 0. 0. 0. 0. 0. 0. 0.
 #30|200|30   Quad  QMQB
1 0. 0. 0.
'CHANGREF'
ZS -0.001                     # remove vertical offset
...
'REBELOTE'                                                                                            1023
199999 0.2 99
'END'                                                                                                 1024
```

The longitudinal spin direction is again not preserved in Fig. 17. Similarly to the dipole roll case, we restore the longitudinal polarization direction by inserting a spin rotator at the beginning of the lattice, which rotates the spin by 2° about the longitudinal axis leaving the orbital motion unaffected. Note that a greater spin rotation angle is used in this case to attain better polarization preservation. This is not a general property of this kind of error but depends on the parameters of the ring, which have not been optimized in this version of the lattice for the spin dynamics in any way. The spin motion with the spin rotator is shown in Fig. 18.

```
...
'SPINR'
1
0.  2.
...
```

3.4 Spin dynamics during acceleration in a figure-8 ring

In this section we simulate the spin dynamics during acceleration in the figure-8 ring. We insert a single zero-length RF cavity with parameters chosen such that it accelerates a proton beam from $G\gamma = 114.5$ ($p = 59.9153$ GeV/c) to $G\gamma = 115.5$ ($p = 60.4387$ GeV/c) in 200,000 turns with a synchronous phase of 20° (see appendix). We first accelerate a particle with initially longitudinal spin on the reference orbit in an ideal figure-8 ring. The longitudinal spin component is plotted versus $G\gamma$ every 100 turns in Fig. 19. Since the figure-8 ring is ideal and the numerical accuracy is adequate, the spin remains longitudinal throughout the acceleration process.

```
Generated by MADX -> Zgoubi translator
'OBJET'                                                                                                  0
199855.9041     # G.gamma=114.5, p=59.91529274 GeV/c, E=59.92263895 GeV
2
1  1
.0 .0 .0 .0 0.  1.  'o'
1
'PARTICUL'                                                                                               1
9.3827203E+02 1.602176487E-19 1.7928474 0 0
'SPNTRK'                                                                                                 2
4
1. 0. 0.
...
'CAVITE'
2
1415.3172372 165.0            # closed orbit length [m], harmonic number
7650.745651 2.79252680319093   # accel. to G.gamma=115.5, p=60.43869817 GeV/c, E=60.44598077 GeV in 200k turns
...
'REBELOTE'                                                                                            1023
199999 0.2 99
'END'                                                                                                 1024
```

```
...
'SPINR'
1
0.  5.
...
```

We next simulated acceleration of a particle in a figure-8 ring with the same 0.2 mrad dipole roll error as discussed in section 3.3.1. The particle with initially longitudinal spin is launched along the reference orbit. As in the earlier study, there is no closed orbit correction. The resulting longitudinal spin component is plotted versus $G\gamma$ every 100 turns in Fig. 20.

To preserve the longitudinal polarization during acceleration, we insert a spin rotator as in the earlier studies, which rotates the spin by 5° about the longitudinal axis. To better understand the spin behavior, we accelerate at the same rate as before for 400,000 turns thus covering twice the energy range, from $G\gamma$ of 114.5 to 116.5. The longitudinal spin component as a function of $G\gamma$ is shown every 200 turns in Fig. 21. The nature of this behavior needs further study and understanding but the dips in the graph probably correspond to the points in energy of stronger zero-harmonic spin resonance strength. Finally, Fig. 22 plots $G\gamma$ and kinetic energy, respectively, from the same simulation as functions of the turn number every 200 turns to confirm that acceleration was simulated correctly.

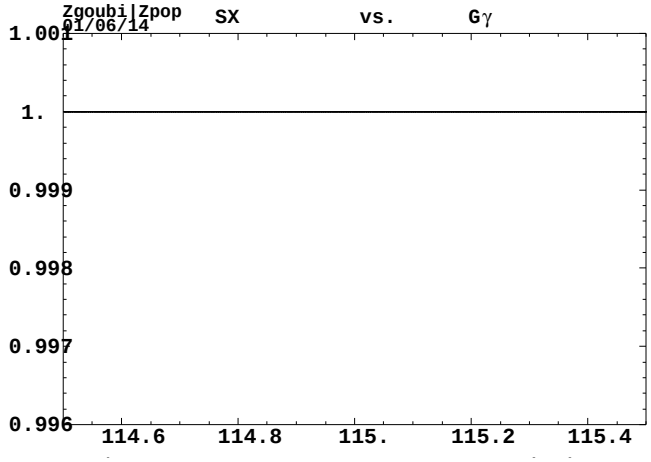

Figure 19: Longitudinal spin component S_x of the particle with $S_x^i = 1$ plotted vs. $G\gamma$ every 100 turns with individual points connected by a solid line. The particle moves along the reference orbit in an ideal ring.

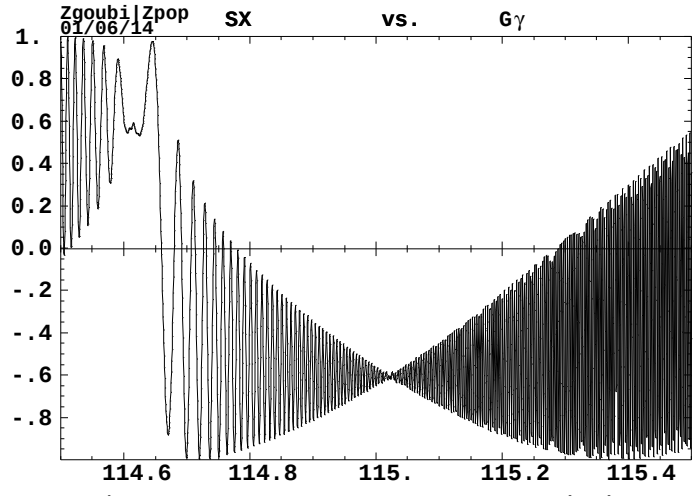

Figure 20: Longitudinal spin component S_x of the particle with $S_x^i = 1$ plotted vs. $G\gamma$ every 100 turns, over 200,000 turns, with individual points connected by a solid line. The particle is initially launched along the reference orbit in a ring with one of the arc dipoles rolled by 0.2 mrad.

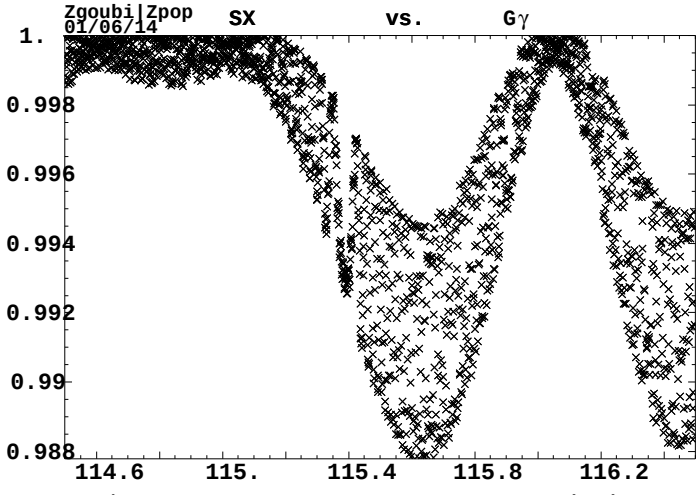

Figure 21: Longitudinal spin component S_x of the particle with $S_x^i = 1$ plotted vs. $G\gamma$ every 200 turns, over 400,000 turns, with The particle is initially launched along the reference orbit in a ring with one of the arc dipoles rolled by 0.2 mrad. The ring contains a spin rotator placed at the launch point, which rotates the spin by 5° about the longitudinal axis.

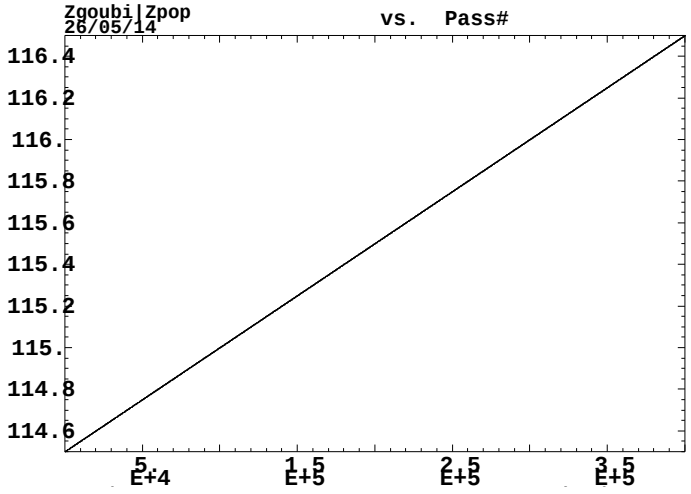

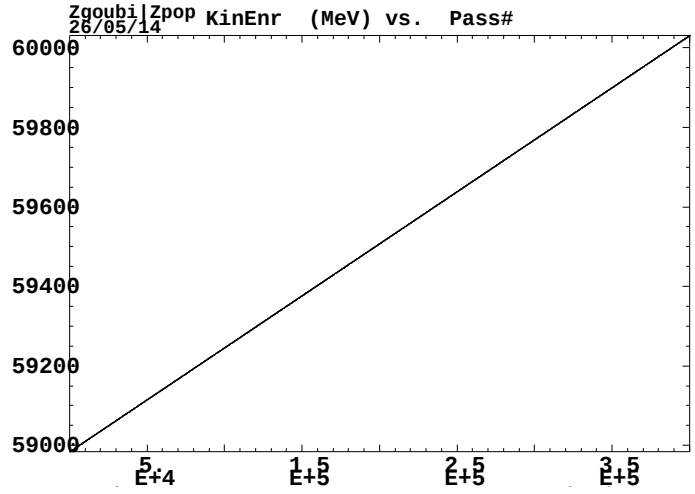

Figure 22: $G\gamma$ (left) and kinetic energy (right) plotted vs. the turn number every 200 turns, over 400,000 turns. The particle is initially launched along the reference orbit in a ring with one of the arc dipoles rolled by 0.2 mrad.

Appendix - Zgoubi input data file

The following lists the top and bottom parts of the Zgoubi input data file for the 60 GeV MEIC proton ring, including acceleration.

The start/end points of the lattice are at one of the two IPs.

The multi-turn tracking is ensured by the 'REBELOTE' keyword at the end of the data list, the acceleration is provided by 'CAVITE' located right above. 'SCALING' in the top part of the data list ensures the ramping of the magnet fields (scaling of the strengths) following the rigidity kick by 'CAVITE'.

```
 Generated by MADX -> Zgoubi translator
'OBJET'
199855.9041     # G.gamma=114.5, p=59.91529274 GeV/c, E=59.92263895 GeV
2
1  1
.0 .0 .0 .0 0.  1.  'o'
1

'PARTICUL'
9.3827203E+02 1.602176487E-19 1.7928474 0 0
'SPNTRK'
4
1. 0. 0.
'FAISCEAU'

'FAISTORE'
b_zgoubi.fai
1
'FAISCEAU'

'SCALING'
1  2
BEND
-1
199.8559041
1
MULTIPOL
-1
199.8559041
1

'MARKER'   MARK      COMPLETE_STAR\$START

'SPINR'
1
0.  5.

'DRIFT'    DRIF      OFFB1
    500.000000
'MULTIPOL' RBEN      RBFFBR
0  .Dip
 100.000000  10.00   0.05996000    0.     0.  0. 0. 0. 0. 0. 0. 0.0
0. 0. 10.00  4.0  0.800 0.00 0.00 0.00 0.00 0. 0. 0. 0.
4  .1455   2.2670  -.6395  1.1558  0. 0.  0.
0. 0. 10.00  4.0  0.800 0.00 0.00 0.00 0.00 0. 0. 0. 0.
4  .1455   2.2670  -.6395  1.1558  0. 0.  0.
   0.  0.  0.  0. 0. 0. 0. 0. 0.
 #30|100|30    Dip  RBFFBR
 3    0. 0.    0. 0.  -2.9980044910E-03
'DRIFT'    DRIF      OFFB2
    100.000000
'MULTIPOL' QUAD      QFFB1
0  .Quad
  120.000000 10.00     0. 00   -0.2637371346 0. 0. 0. 0. 0. 0. 0.0
0. 0. 6.00  3.00 1.00 0.00 0.00 0.00 0.00 0. 0. 0. 0.
6  .1122 6.2671 -1.4982 3.5882 -2.1209 1.723
0. 0. 6.00  3.00 1.00 0.00 0.00 0.00 0.00 0. 0. 0. 0.
6  .1122 6.2671 -1.4982 3.5882 -2.1209 1.723
 0. 0. 0. 0. 0. 0. 0. 0. 0. 0.
 #30|480|30   Quad  QFFB1
1 0. 0. 0.
'DRIFT'    DRIF      OFFB3
    100.000000
'MULTIPOL' QUAD      QFFB2
0  .Quad
  240.000000 10.00     0. 00    0.1520851633 0. 0. 0. 0. 0. 0. 0. 0.0
0. 0. 6.00  3.00 1.00 0.00 0.00 0.00 0.00 0. 0. 0. 0.
6  .1122 6.2671 -1.4982 3.5882 -2.1209 1.723
0. 0. 6.00  3.00 1.00 0.00 0.00 0.00 0.00 0. 0. 0. 0.
6  .1122 6.2671 -1.4982 3.5882 -2.1209 1.723
 0. 0. 0. 0. 0. 0. 0. 0. 0. 0.
 #30|960|30   Quad  QFFB2
1 0. 0. 0.
'DRIFT'    DRIF      OFFB4
    100.000000
'MULTIPOL' QUAD      QFFB3
0  .Quad
  120.000000 10.00     0. 00   -0.1058604401 0. 0. 0. 0. 0. 0. 0. 0.0
0. 0. 6.00  3.00 1.00 0.00 0.00 0.00 0.00 0. 0. 0. 0.
6  .1122 6.2671 -1.4982 3.5882 -2.1209 1.723
0. 0. 6.00  3.00 1.00 0.00 0.00 0.00 0.00 0. 0. 0. 0.
6  .1122 6.2671 -1.4982 3.5882 -2.1209 1.723
 0. 0. 0. 0. 0. 0. 0. 0. 0. 0.
 #30|480|30   Quad  QFFB3
1 0. 0. 0.
'DRIFT'    DRIF      OFFB5
    399.500000
'DRIFT'    DRIF      OFFB5_
      0.500000
'MULTIPOL' RBEN      SBFFBR
0  .Dip
 400.000000  10.00  -0.14997750    0.     0.  0. 0. 0. 0. 0. 0. 0.0
0. 0. 10.00  4.0  0.800 0.00 0.00 0.00 0.00 0. 0. 0. 0.
4  .1455   2.2670  -.6395  1.1558  0. 0.  0.
0. 0. 10.00  4.0  0.800 0.00 0.00 0.00 0.00 0. 0. 0. 0.
4  .1455   2.2670  -.6395  1.1558  0. 0.  0.
   0.  0.  0.  0. 0. 0. 0. 0. 0.
 #30|400|30    Dip  SBFFBR
 3    0. 0.    0. 0.   3.0000000000E-02
'DRIFT'    DRIF      OFFB6_
      0.500000
'DRIFT'    DRIF      OFFB6
    399.500000
'DRIFT'    DRIF      OFFB7
    400.000000
 %
 -
 %
'DRIFT'    DRIF      OFFB2_US
     50.000000
'MULTIPOL' QUAD      QFFB1_US
0  .Quad
  120.000000 10.00    0.0000000000   -0.4290012400 0.0 0.0 0.0 0.0 0.0 0.0 0.0 0.0
0. 0. 6.00  3.00 1.00 0.00 0.00 0.00 0.00 0. 0. 0. 0.
6  .1122 6.2671 -1.4982 3.5882 -2.1209 1.723
0. 0. 6.00  3.00 1.00 0.00 0.00 0.00 0.00 0. 0. 0. 0.
6  .1122 6.2671 -1.4982 3.5882 -2.1209 1.723
 0. 0. 0. 0. 0. 0. 0. 0. 0. 0.
 #30|480|30   Quad  QFFB1_US
1 0. 0. 0.
'DRIFT'    DRIF      OFFB1_US
360.000000

'CAVITE'
2
1415.3172372 165.0           # closed orbit length [m], harmonic number
7650.745651 2.79252680319093 # accel. to G.gamma=115.5, p=60.43869817 GeV/c,
                             # E=60.44598077 GeV in 200k turns
'MARKER'   COMPLETE_STAR\$END
'FAISCEAU'
'SPNPRT'
'REBELOTE'
399999 0.2 99
'END'
```

References

[1] F. Lin, MEIC Project at Jefferson Lab, EIC14 workshop, March 17-21, 2014, Thomas Jefferson National Accelerator Facility, Newport News, VA. http://appora.fnal.gov/pls/eic14/agenda.full.

[2] F. Méot, Zgoubi Users' Guide, Report C-A/AP/470, BNL C-AD, October 2012. The code, guide, examples, zpop data treatment software, toolbox, are available at http://sourceforge.net/p/zgoubi/code/HEAD/tree/.

[3] Zgoubi toolbox can be downloaded from the "trunk" folder at http://sourceforge.net/p/zgoubi/code/HEAD/tree/. It provides various software such as a translator from MADX (or MAD8) twiss type of files to Zgoubi input data file, closed orbit search, dynamic aperture search, spin $\vec{n}_0$ search, spin distribution or spin tune computation, graphic interfaces, and a lot more.

[4] Ya.S. Derbenev *et al.*, *"Ion polarization control in MEIC rings using small magnetic field integrals"*, in Proc. of PSTP 2013, Charlottesville, VA).